1990

A Computer Simulation of the Oxygen Reduction Reaction in Carbonate Melts

P. K. Adanuvor
Texas A & M University - College Station

Ralph E. White
University of South Carolina - Columbia, white@cec.sc.edu

A. J. Appleby
Texas A & M University - College Station

Publication Info

Journal of the Electrochemical Society, 1990, pages 2095-2103.

DOI: 10.1149/1.2086891
http://dx.doi.org/10.1149/1.2086891

S^*_i	transported entropy for component i, $J\ K^{-1}\ F^{-1}$
$S^*_{MX\|Y}$	entropy transported at contact MX|Y, $J\ K^{-1}\ F^{-1}$
T_i	temperature of compartment, i, K
t_i	transference number of constituent i, C^{-1}
t	time, s
u_i	partial molar energy of component i, $J\ mol^{-1}$
$(dU/dt)_{tot}$	total internal energy change per unit time of the system, $J\ s^{-1}$
$(du/dt)_{el}$	rate of energy change at electrodes due to chemical processes, $J\ s^{-1}$
$(du/dt)_{jnct}$	rate of energy change of junction due to chemical processes, $J\ s^{-1}$
V_i	partial molar volume of component i, m^3
x	coordinate, m
α'	temperature coefficient of ϵ', $V\ K^{-2}$
α	temperature coefficient of ϵ°, $V\ K^{-2}$
ϵ'	apparent thermoelectric power, $V\ K^{-1}$
ϵ°	thermoelectric power for $\Delta T = 0$ at T, $V\ K^{-1}$
μ_i	molar chemical potential of component i, $J\ mol^{-1}$
τ_i	Thomson coefficient of component i, $J\ K^{-1}\ F^{-1}$

REFERENCES

1. Y. Ito, H. Kaiya, S. Yoshizawa, S. K. Ratkje, and T. Førland, *This Journal*, **131,** 2504 (1984).
2. T. Jacobsen and G. J. Bores, *ibid.*, **124,** 207 (1977); *ibid.*, **124,** 210 (1977).
3. J. N. Agar, in "Advances in Electrochemistry and Electrochemical Engineering," Vol. 3, P. Delahay, Editor, Interscience, New York (1963).
4. S. Shibata and M. P. Sumino, *J. Electroanal. Chem.*, **193,** 135 (1985); T. Ozeki and S. Hikine, *ibid.*, **195,** 71 (1985).
5. H. G. Hertz and S. K. Ratkje, *This Journal*, **136,** 1691, 1998 (1989).
6. R. Haase, *Electrochim. Acta*, **31,** 545 (1986).
7. D. D. Macdonald, A. C. Scott, and P. Wentreck, *This Journal*, **126,** 1618 (1979).
8. P. R. Tremaine, N. H. Sagert, and G. J. Wallace, *J. Phys. Chem.*, **85,** 1977 (1981).
9. Y. D. Rakhmilevich, I. A. Dibrov, and S. N. L'vov, *Zh. Fiz. Khim.*, **58,** 2019 (1984) and **61,** 2391 (1987).
10. Y. D. Rakhmilevich, M. M. Suprun, S. N. L'vov, and I. A. Dibrov, *ibid.*, **61,** 554 (1987).
11. Y. D. Rakhmilevich, I. A. Dibrov, and S. N. L'vov, *ibid.*, **61,** 2391 (1987).
12. H. G. Hertz, "Electrochemistry," Springer-Verlag, Berlin (1980).
13. T. Førland, L. U. Thulin, and T. Østvold, *J. Chem. Ed.*, **48,** 741 (1971).
14. K. S. Førland, T. Førland, and S. K. Ratkje, "Irreversible Thermodynamics," Wiley: Chichester, England (1988).
15. H. S. Harned and B. B. Owen, "The Physical Chemistry of Electrolytic Solution," 3rd ed., Reinhold Pub. Corp., New York (1955).
16. D. Ives and G. Janz, "Reference Electrodes," Academic Press, Inc., New York (1961).
17. R. Haase and H. Schönert, *Z. Phys. Chem.*, **25,** 193 (1960).
18. International Critical Tables, Vol. 6, p. 214 (1929).
19. V. B. Parker, "Thermal Properties of Aqueous Uni-Univalent Electrolytes," National Bureau Standard Reference Data, Series NBS 2, Washington, DC (1965).
20. D. Wagman, H. Evans, V. B. Parker, H. Schumm, J. Halow, M. Bailey, K. L. Churney, and R. L. Nuttall, *J. Phys. Chem. R. Data* II, Suppl. 2 (1982).
21. "Standard Potentials in Aqueous Solutions," A. J. Bard, R. Parsons, and J. Jordan, Editors (1985).
22. R. Triolo, L. Blum, and A. M. Floriano, *J. Phys. Chem.*, **82,** 1368 (1978).
23. N. Takeyama and K. Nakashima, *J. Soln. Chem.*, **17,** 305 (1988).

A Computer Simulation of the Oxygen Reduction Reaction in Carbonate Melts

P. K. Adanuvor,* R. E. White,* and A. J. Appleby*

Center for Electrochemical Systems and Hydrogen Research, Texas Engineering Experiment Station, Texas A&M University, College Station, Texas 77843

ABSTRACT

A computer simulation of the oxygen reduction reaction in various carbonate melts has been carried out under steady-state conditions on the basis of a proposed kinetic model which takes into consideration the autocatalytic reaction involving oxygen and other reducible oxygen species in the melt, and the neutralization of oxide ions by dissolved carbon dioxide. A simulation of the presence of (physically) dissolved oxygen, in the diffusion layer region of the melt, corresponding to the possible situation in porous electrodes, causes a significant enhancement in the polarization curves, particularly in the mass-transfer control region. On the other hand, high levels of dissolved CO_2 in the melt reduce the current density in the mass-transfer control region by reducing the concentration of active dioxygen ions, but enhance it considerably in the kinetic limiting (CO_2 neutralization) region. High rates of the autocatalytic and neutralization reactions display the same effects on the polarization curves as dissolved O_2 and CO_2, respectively, but to a lesser degree. Comparison of the simulated polarization curves in various carbonate melts indicates that Li-rich melts show the best kinetic performance. On the contrary, the highest limiting currents are observed in K- or Na-rich melts. Variation of the cation composition in Li/K carbonate melts indicates that melts of high Li-content should give better kinetic performance.

The development of the molten carbonate full cell (MCFC) has been hindered partly by problems associated with the oxygen cathode. The severe material problems associated with the oxygen reaction, particularly at the high operating temperatures (>600°C) of the MCFC, the complexity of the O_2 reduction reaction and the polarization losses caused by the slow kinetics of this reaction are some of the crucial problems that have to be resolved in order to develop an effective and efficient oxygen cathode as an integral part of the MCFC. The basis for resolving these problems lies in the elucidation of the kinetics of the cathode reaction.

Efforts to elucidate the kinetics of the oxygen cathode in the MCFC have been in progress since the early 1970s. However, to date, the actual nature of the reaction mechanism has not been fully resolved. Appleby and Nicholson gave evidence that (1-4) oxygen dissolves in alkali carbonate melts primarily as a mixture of peroxide ($O_2^{=}$) and superoxide (O_2^-) ions; the relative amounts of these ions depend strongly on the composition of the alkali carbonate melt. The presence of peroxide ions has been confirmed in pure Li_2CO_3 or Li-rich melts (2); whereas

* Electrochemical Society Active Member.

superoxide ions have been observed to be the dominant species in K- or Na-rich melts (3-5). Evidence for this is provided by the thermodynamic studies of chemical equilibria in alkali carbonate melts (7). As a consequence of this, two reaction mechanisms based on the presence of the peroxide and superoxide species in the melt have generally been postulated for oxygen reduction in alkali carbonate melts (8, 9)

Peroxide mechanism

$$1/2\ O_2 + CO_3^= \rightleftharpoons O_2^= + CO_2$$

$$O_2^= + e^- \rightleftharpoons O^= + O^-$$

$$O^- + e^- \rightleftharpoons O^=$$

$$2\ O^= + 2CO_2 \rightleftharpoons 2CO_3^=$$

Superoxide mechanism

$$3/4\ O_2 + 1/2\ CO_3^= \rightleftharpoons O_2^- + 1/2\ CO_2$$

$$O_2^- + e^- \rightleftharpoons O_2^=$$

$$O_2^= + 2e^- \rightleftharpoons 2\ O^=$$

$$2\ O^= + 2CO_2 \rightleftharpoons 2CO_3^=$$

In addition, a third mechanism, "the percarbonate mechanism," based on the hypothetical percarbonate ion, has occasionally been considered in the literature (8, 9). However, none of these mechanisms has been found to be unambiguously consistent with experimental results, especially those from porous electrodes.

Conflicting conclusions persist in the literature about the dominant species in alkali carbonate melts, the true nature of the reaction mechanisms, and the values of the kinetic parameters. For example, Appleby and Nicholson (4) considered that peroxide and superoxide ions are reduced successively by a $2e^-$ and a $1e^-$ step in Li/K and Na/K carbonate melts whereas Vogel *et al.* (6) concluded that the reduction appears to be complete in a single superoxide wave by a $3e^-$ process in Li/K melt. The exchange current densities evaluated by Lu (10), Yuh (8), and Uchida *et al.* (11) for the O_2 reduction reaction at a gold electrode in Li/K melt by the potential-step method were two orders of magnitude greater than the values obtained by Appleby and Nicholson (4) using potential sweep. The reported reaction orders for O_2 and CO_2 also vary (5, 12-14). Yuh (8) found the oxygen cathode to be under mixed reaction control, while other investigators have analyzed their results either in terms of a fully reversible process (3, 11, 15) or as one with completely irreversible kinetics (6, 7, 16). The reason for the conflicting results can partly be attributed to the basic assumptions made in analysis of the results. For example, even if the peroxide or superoxide ion is the dominant species in the melt, both species should be taken into consideration in the analysis of the results, since they may be involved successively. Similarly, completely reversible or irreversible kinetics should not be applied in the analysis of the results when mixed kinetics may best describe the data.

The complexity of the sequence of reactions at the O_2 cathode makes the traditional approach of deciphering the kinetics of this reaction system solely via experimentation very cumbersome. Computer simulation provides a rapid and direct way of gaining insight into the behavior of such a complex reaction system. Digital simulation can complement experimentation by (*i*) defining *a priori* the parameters necessary for the efficient design of experiments, and by (*ii*) serving as an important diagnostic tool in the analysis and interpretation of experimental data.

In this paper, the reaction sequences for oxygen reduction in MCFC are simulated under conditions similar to those employed experimentally using bulk melts. The simulations were carried out at a rotating disk electrode (RDE), primarily because of its well-defined hydrodynamics and ease of modeling (17). The conditions in a porous electrode are simulated by allowing the effective molecular dioxygen concentration to vary outside the diffusion layer to simulate a gas atmosphere. Therefore, the objectives of this work are to predict (i) the effect of the autocatalytic and the neutralization reactions on the polarization curves, (*ii*) the effect of different cations and their compositions in the melt on the polarization data, and (*iii*) the effects of dissolved gases (molecular oxygen and carbon dioxide) on the steady-state polarization currents.

Model Development

Kinetic model.—The kinetic model combines the $2e^-$ reduction of $O_2^=$ with the $1e^-$ reduction of O_2^- ions proposed by Appleby and Nicholson (3, 4). The first step in this model involves the chemical dissolution of oxygen in the melt to form peroxide ($O_2^=$ and superoxide (O_2^-) ions, as in equilibrium reactions [1] and [2] at the gas-melt interface

$$1/12\ [O_2 + 2CO_3^= \rightleftharpoons 2\ O_2^= + 2CO_2] \quad [1]$$

$$1/6\ [O_2 + O_2^= \rightleftharpoons 2\ O_2^-] \quad [2]$$

$$2/3\ [O_2^- + e^- \rightleftharpoons O_2^=] \quad [3]$$

$$2/3\ [O_2^= + 2e^- \rightleftharpoons 2\ O^=] \quad [4]$$

$$1/6\ [3/2\ O_2 + O^= \rightleftharpoons 2\ O_2^-] \quad [5]$$

$$7/6\ [O^= + CO_2 \rightleftharpoons CO_3^=] \quad [6]$$

$$1/2\ O_2 + CO_2 + 2e^- \rightleftharpoons CO_3^= \quad [7]$$

It must be noted that the sum of reactions [1] and [2] leads to the usual representation of the superoxide formation reaction in Eq. [2A]

$$1/12\ [3\ O_2 + 2CO_3^= \rightleftharpoons 4\ O_2^- + 2CO_2] \quad [2A]$$

The $O_2^=$ and O_2^- species formed at the electrolyte-gas interface then diffuse to the electrode surface where they are reduced by the electrochemical reactions in Eq. [3] and [4]. The oxide ions ($O^=$) formed in reaction [3] can be neutralized by dissolved CO_2 in the melt according to reaction [6]. However, this neutralization reaction has been found to be slow and may possibly be rate limiting (10). Therefore, a buildup of $O^=$ ions in the vicinity of the electrode may occur leading to changes in the acid-base properties of the melt and, consequently, to changes in the local electrode potential (2-4). A presence of dissolved oxygen (O_2) in the melt can lead to an autocatalytic reaction involving dissolved oxygen and a reducible oxygen species such as $O^=$ in the melt as represented by Eq. [5]. There is as yet no evidence to support the presence of dissolved oxygen in bulk melts (1, 5). However, the situation may be quite different in porous electrodes where the dissolution zone for molecular oxygen in the melt could extend into the thin electrolyte film/meniscus in contact with the catalyst layer. For the bulk melt case, it is assumed that all of the oxygen that dissolves in the melt reacts immediately with the melt according to Eq. [1] and [2] at the melt-gas interface, so that no dissolved oxygen would exist in the reaction zone. Both this case, as well as the more general case where some unreacted dissolved oxygen exists in the bulk electrolyte which perhaps occurs in porous electrodes, are considered here. The sum of the sequence of reactions in Eq. [1]-[6] yields the half-cell reaction in Eq. [7] for the overall reduction of oxygen in the molten carbonate fuel cell.

The model equations for the kinetic rate processes are given below. Reactions [1] and [2] are assumed to be very rapid and therefore, they can be represented by the equilibrium expressions in Eq. [8] and [9], respectively

$$K_1 = \frac{p_{CO_2}^2 c_{O_2^=}^2}{p_{O_2} c_{CO_3^=}^2} \quad [8]$$

$$K_2 = \frac{c_{O_2^-}^2}{p_{O_2} c_{O_2^=}^2} \quad [9]$$

The homogeneous reactions occurring in melt are represented by the following rate equations

$$r_5 = -k_{f(5)} c_O = c_{O_2}^{3/2} + k_{b(5)} c_{O_2^-}^2 \quad [9]$$

$$r_6 = -k_{f(6)} c_O = c_{CO_2} + k_{b(6)} c_{CO_3^=} \quad [10]$$

where the net rate of consumption/production of a species i involved in the homogeneous reactions is denoted by

$$R_i = \sum_j s_{i,j} r_j \quad [11]$$

The derivation of the kinetic rate expressions for the electrochemical reactions in Eq. [3] and [4] is given in the Appendix. The rate equations for these two reactions are given by Eq. [A-22] and [A-24]

$$i_3 = i_{o3,ref}\left[\left(\frac{c_{O_2^{=},0}}{c_{O_2^{=},ref}}\right)^2 \exp\left(\frac{\alpha_{a,3}\mathbf{F}}{RT}\eta_4\right) - \left(\frac{c_{O_2^{=},0}}{c_{O_2^{=},ref}}\right)\exp\left(\frac{-\alpha_{c,3}\mathbf{F}}{RT}\eta_3\right)\right] \quad [A\text{-}22]$$

$$i_4 = i_{o4,ref}\left[\left(\frac{c_{O^{=},o}}{c_{O^{=},ref}}\right)\exp\left(\frac{\alpha_{a,4}\mathbf{F}}{RT}\eta_3\right) - \left(\frac{c_{O_2^{=},o}}{c_{O_2^{=},ref}}\right)\exp\left(\frac{-\alpha_{c,4}\mathbf{F}}{RT}\eta_4\right)\right] \quad [A\text{-}24]$$

The overall current density is the sum of the partial current densities in Eq. [A-22] and [A-24], that is

$$i = i_3 + i_4 \quad [12]$$

The above rate expressions are assumed to occur in K-rich or Na-rich carbonate melts such as Li/K, Li/Na/K, Li/Na, and Na/K, in which both $O_2^{=}$ and O_2^{-} species are known to exist (7). On the contrary, only $C_2^{=}$ species have been established to be present in Li_2CO_3 melts (2). Therefore, the following reaction sequence was proposed for Li_2CO_3

$$1/3[O_2 + 2CO_3^{=} \rightleftharpoons 2\,O_2^{=} + 2CO_2] \quad [1]$$

$$[O_2^{=} + 2e^- \rightleftharpoons 2\,O^{=}] \quad [4]$$

$$1/3[O_2 + 2\,O^{=} \rightleftharpoons 2\,O_2^{=}] \quad [5\text{-}A]$$

$$5/3[O^{=} + CO_2 \rightleftharpoons CO_3^{=}] \quad [6]$$

$$1/2\,O_2 + CO_2 + 2e^- \rightleftharpoons CO_3^{=} \quad [7]$$

Material balance equations at the RDE.—A mass balance on species i within the diffusion layer of a RDE yields (18)

$$\frac{\partial c_i}{\partial t} = -\nabla \cdot \mathbf{N}_i + R_i \quad [13]$$

where the flux of species i is given by the sum of the migration, the diffusion, and the convection terms

$$\mathbf{N}_i = -z_i u_i \mathbf{F} c_i \nabla\Phi - D_i \nabla c_i + c_i \mathbf{v} \quad [14]$$

Substitution of the y-component of $\mathbf{N}_i$ in Eq. [14] into Eq. [13] with further simplification (17, 18) leads to the final one-dimensional material balance equation

$$\frac{\partial c_i}{\partial t} = \frac{D_i}{\delta_D^2}\frac{\partial^2 c_i}{\partial \xi^2} + \frac{3D_R\xi^2}{\delta_D^2}\frac{\partial c_i}{\partial \xi} + \frac{z_i\mathbf{F}}{\delta_D^2}\frac{D_i}{RT}\left(\frac{\partial\Phi}{\partial\xi}\frac{\partial c_i}{\partial\xi} + c_i\frac{\partial^2\Phi}{\partial\xi^2}\right) + R_i \quad [15]$$

where R_i has been defined previously. The dimensionless distance is defined as

$$\xi = y/\delta_D \quad [16]$$

where y is the normal distance from the electrode surface, and δ_D is the diffusion layer thickness which is related to the rotation speed of the electrode by the relation (18)

$$\delta_D = \left(\frac{3D_R}{a\nu}\right)^{1/3}\left(\frac{\nu}{\Omega}\right)^{1/2} \quad [17]$$

The initial conditions are

$$\text{at } t = 0 \text{ and } \xi \geq 0\ c_i = c_{i,bulk} \text{ and } \Phi = \Phi_{re} \quad [18]$$

and the boundary conditions are as follows

$$\text{at } \xi = 2 \text{ and } t > 0\ c_i = c_{i,bulk} \text{ and } \Phi = \Phi_{re} \quad [19]$$

where $c_{i,bulk}$ is assumed to be equal to $c_{i,ref}$. At the electrode surface

$$\text{for } t > 0, \text{ as } \xi \rightarrow 0,\ \Phi \rightarrow \Phi_o, \text{ and}$$

$$\frac{1}{\delta_D}\left[D_i\frac{dc_i}{d\xi} + z_i c_i \mathbf{F}\frac{D_i}{RT}\frac{d\Phi}{d\xi}\right]_{|\xi=o} = \sum_{j=1}^{m}\frac{s_{i,j}i_j}{n_j\mathbf{F}} \quad [20]$$

Steady-state results are obtained by equating the left-hand side of Eq. [13] to zero, that is

$$\frac{\partial c_i}{\partial t} = 0 \quad [21]$$

The bulk concentration of dissolved O_2 and CO_2 in the melt is determined by Henry's law

$$c_i = H_i p_i \quad [22]$$

whereas the bulk concentrations of O_2^{-} and $O_2^{=}$ species formed by the chemical dissolution of O_2 in the melt are determined by the equilibrium relations established in Eq. [8] and [9] (5, 6). The bulk concentration of $O^{=}$ species is calculated from Eq. [6] under equilibrium conditions.

Thermodynamic information on the standard electrode potentials for the electrochemical reactions and the equilibrium constants for the chemical reactions were obtained from the free energy calculations for these reactions. The electrode potential of the reference oxygen electrode (33% O_2:67% CO_2 mixture) at 750°C in various carbonate melts was calculated from the free energies of formation (19). The free energy changes (and therefore the equilibrium constants) of the reactions

$$M_2O + 1/2\,O_2 = M_2O_2 \text{ or } O^{=} + 1/2\,O_2 = O_2^{=} \quad [23]$$

$$M_2O_2 + O_2 = 2MO_2 \text{ or } O_2^{=} + O_2 = 2\,O_2^{-} \quad [24]$$

$$1/2\,M_2O + 3/4\,O_2 = MO_2 \text{ or } 1/2\,O^{=} + 3/4\,O_2 = O_2^{-} \quad [25]$$

$$2/3\,M_2O + 2/3\,MO_2 = M_2O_2 \text{ or } 2/3\,O^{=} + 2/3\,O_2^{-} = O_2^{=} \quad [26]$$

(where M stands for Li, K, or Na) were calculated using the free energy data from the JANAF tables (19) (assuming the ideal mixing rule). Next, the standard electrode potentials for the electrochemical reactions were calculated with respect to the reference oxygen electrode in the same melt. The free energies of MO_2, M_2O_2, and M_2O in the liquid state are not available and therefore, the solid-state values were used as an approximation. The free energy of formation of LiO_2 is also not available. It was estimated from the solubility data of oxygen in fused Li/K carbonate (20) as −184.87 KJ/mol at 1023.15 K. The validity of this value was checked by applying the fact that if a ternary compound lies on a known pseudo-binary tie line within a ternary system, it could be possible to extract that compound's minimum or maximum allowable free energy from the free energies of the two other compounds lying along the same pseudo-binary tie line (20). From Eq. [23] and [25], with M = Li, the maximum and minimum allowable free energies of formation were estimated as −158.23 and −207.16 KJ/mol. The estimated value of −184.87 KJ/mol lies within this range.

The solution of the model equations was carried out by casting the governing equations in the finite difference form and solving the resulting algebraic equations by Newman's technique (21). The solution yields the potential and the concentration profiles of reacting species in the diffusion layer, and the partial current densities at the electrode surface.

Results and Discussion

Table I lists the thermodynamic and kinetic parameter values used in the simulation. Figure 1 shows a plot of the

Table I. Thermodynamic properties and kinetic parameters for model simulation

Parameters	Carbonate mixture					
	Li:K (62:38)	Li:Na:K (45.5:31.5:25)	Na:K (43:57)	Na:K (56:44)	Li:Na (52:48)	Li
$K_1 \times 10^{16}$ (atm)	19.65	5.22	0.007	0.014	55.04	11,500
$K_2 \times 10^5$ (mol/cm^3/atm)	3.40	1.55	7.68	3.53	0.42	0.53
$K_5 \times 10^4$ (mol/cm^3/atm$^{3/2}$)	0.082	0.098	43.47	12.89	1.57	1.7×10^{-4}
$K_6 \times 10^{-8}$ (atm^{-1})	0.34	1.12	701	329	0.11	6.9×10^{-4}
U^0_{re} (V)	2.61	2.52	2.34	2.34	2.55	2.76
U^0_3 (V)	1.90	1.73	1.06	1.11	1.93	2.52
U^0_4 (V)	1.93	1.87	1.54	1.58	1.99	2.25
$\alpha_{c,3}$	1.00	1.00	1.00	1.00	1.00	1.00
$\alpha_{c,4}$	0.50	0.50	0.50	0.50	0.50	0.50
$i_{o3,ref}$ (mA/cm^2)	24.98	24.98	24.98	24.98	24.98	8.98
$i_{o4,ref}$ (mA/cm^2)	6.31	6.31	6.31	6.31	6.31	—
n_3	2	2	2	2	2	2
n_4	1	1	1	1	1	1
Solution properties	Li^+	K^+	Na^+	$CO_3^=$	$O^=$	$O_2^=$
$D_i \times 10^5$ (cm^2/s)	1.10	1.31	1.20	0.91	1.10	1.12
Solution properties	O_2^-	CO_2	O_2			
$D_i \times 10^5$ (cm^2/s)	1.20	0.99	1.12			
$H_i \times 10^7$ (mol/cm^3/atm)	—	117	2.23			
$\nu = 0.011$ cm^2/s, $T = 1023$ K, $\Omega = 1600$ rpm, $\rho_o = 1.96$ g/cm^3						
Gas composition	O_2	CO_2				
p_i (atm)	0.90	0.10				

current density *vs.* the applied potential in the steady state, in the absence of dissolved molecular O_2 in the diffusion layer region. The contribution to the total current due to the reduction of $O_2^=$ and O_2^- species in the melt is reflected in the partial current density plots in Fig. 1. The dashed curve represents the $2e^-$ reduction of $O_2^=$ species and the dotted curve represents the $1e^-$ reduction of O_2^- species. The net current density (the solid line) is the sum of the two reactions, which is the same as the $3e^-$ reduction of O_2^- to $O^=$. The current density due to the reduction of $O_2^=$ by reaction [4] in the limiting region is about twice that due to the reduction of O_2^- by the $1e^-$ process in reaction [3]. The predominant diffusing species in this melt calculated from the equilibrium relations established in Eq. [1] and [2] is the O_2^- species. Assuming the diffusion coefficient for O_2^- to be the same as that for $O_2^=$ ions, then one would expect the limiting current density of reaction [3] to be greater than

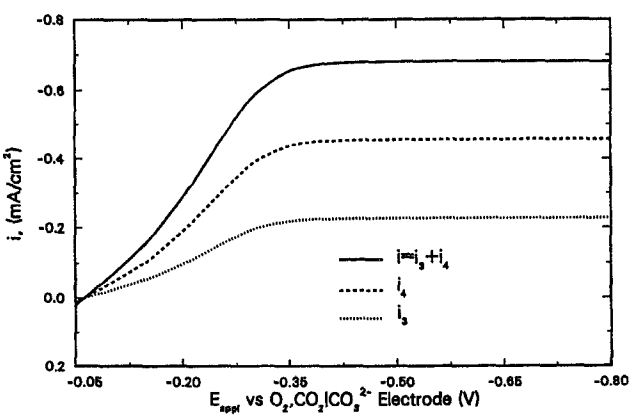

Fig. 1. Steady-state polarization curves in the absence of physically dissolved oxygen in (62:38) Li/K carbonate melt.

that for reaction [4]. However, the reverse situation occurs in this case, as confirmed by the partial current density plots in Fig. 1. This suggests that either O_2^- is acting as a reservoir for $O_2^=$ species or the product $O_2^=$ species of reaction [3] reacts further at more negative potentials to enhance the limiting current of the peroxide reaction. It is likely that both processes might be taking place. Appleby and Nicholson (3, 4) concluded from the analysis of potential scan results in Na/K melt that the $O_2^=$ species produced by the partial reduction of O_2^- ions in Eq. [3] are not reduced further to $O^=$ because of the accumulation of the latter species in the vicinity of the electrode, with consequent shift in the local electrode potential. The accumulation of $O^=$ ions in the vicinity of the electrode in this melt was attributed to the slow neutralization reaction in Eq. [6]. While this seems to be the case under unsteady-state conditions, in the steady state there is sufficient time for neutralization to take place at least in Li/K melt.

The experimental results of Vogel *et al.* (6) suggest that reduction of O_2 in 62:38 Li/K carbonate melt occurs predominantly by the reduction of O_2^- ions in a single wave. These authors interpreted their results (6) in terms of a complete reduction of O_2^- ions by a $3e^-$ process in a single wave, corresponding to the solid curve in Fig. 1. However, the likelihood of O_2^- species being reduced by a $3e^-$ process in a single step is remote. Therefore, a multi-step electrode process such as that outlined in this work (reactions [3] and [4]) is more appropriate.

The presence of dissolved molecular O_2 outside the diffusion layer region of the melt, corresponding to a possible porous electrode model, significantly enhances the cathodic currents particularly in the mass-transfer limiting region. In Fig. 2, the ratio of the limiting current in the presence and absence of simulated dissolved molecular oxygen for the electrode reactions in Eq. [3] and [4], respectively, is approximately the same. This indicates that physically dissolved oxygen in the melt influences the reduction of both $O_2^=$ and O_2^- species to the same extent. Figure 3

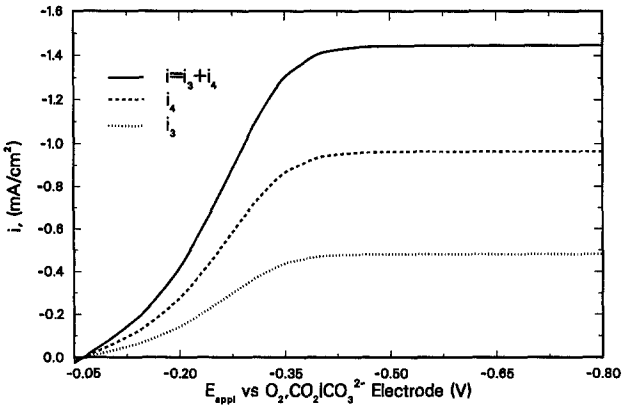

Fig. 2. Steady-state polarization curves in the presence of physically dissolved oxygen in (62:38) Li/K carbonate melt. ($H_{O_2} = 10^{-7}$ mol/atm/cm³).

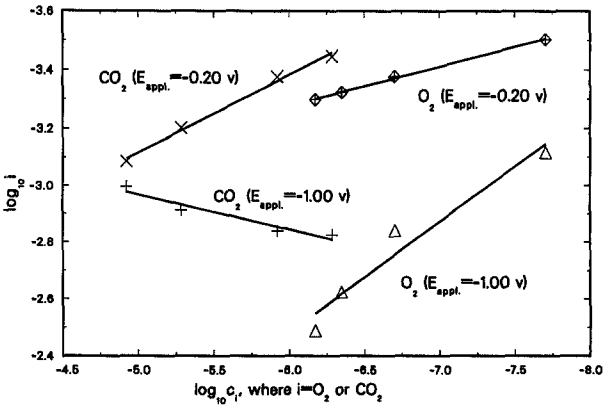

Fig. 4. Logarithmic plot of current density *vs.* concentration of dissolved gases in the near-equilibrium and mass-transfer limiting regions.

shows the steady-state current density change as the simulated Henry's law constant for oxygen is allowed to vary outside of the diffusion region. The higher the concentration of dioxygen outside of the diffusion layer region, the greater the reduction current. The observed enhancement in reduction currents with increase in the partial pressure of oxygen above the melt (4, 10, 22) is attributed to the effect of chemical dissolution of oxygen. On the other hand, a comparison between shielded and unshielded working electrodes has shown that the enhancement of the reduction current can be attributed to a direct reduction of oxygen through the meniscus/film on the unsheathed electrode (22). These results emphasize the significance of physically dissolved, unreacted oxygen in the diffusion layer region of the melt, which may be particularly important in porous electrodes.

Figure 4 shows a plot of predicted values of log current density *vs.* the concentration of the dissolved gases (O_2 and CO_2) in the near-reversible ($E_{appl.} = -0.2$V) and mass-transfer limiting regions ($E_{appl.} = -1.00$V). The slopes of the lines for oxygen are +0.39 in the near-reversible region and +0.14 in the mass-transfer limiting region. The small positive reaction order with respect to oxygen is in agreement with some experimental results in carbonate melts (3, 10); however, it should be noted that the claim that the slope is constant in Fig. 4 for oxygen reduction in the mass-transfer limiting region is speculative.

Reaction orders of +0.27 and −0.12 are shown for CO_2 in the near-reversible and limiting current regions in Fig. 4. This is in agreement with Appleby's and Nicholson's (3) experimental observations of a negative slope and positive slopes in the high and low over-potential regions, respectively, in ternary Li/Na/K and in binary Na/K carbonate melts for peak current *vs.* CO_2 partial pressure.

Figure 5 shows the effect of changing the concentration of dissolved carbon dioxide on the steady-state polarization curves. The polarization current is enhanced significantly in the near-reversible region as the concentration of CO_2 in the melt increases. However, in the mass-transfer controlled region, the limiting current density decreases with a rise in the concentration of dissolved CO_2. The opposite effect is observed when the CO_2 concentration in the melt decreases. Lu (10) reported that feed gases with low CO_2 or low O_2 content will tend to cause high overpotentials at the cathode. This observation is in agreement with the results in Fig. 5. The simulated polarization curves in the presence of dissolved CO_2 can be explained by increasing the neutralization rate of oxide ions according to reaction [6] as CO_2 concentration is allowed to increase. The neutralization of oxide ions decreases the basicity of the melt and results in a shift of the reduction potential of reaction [4] to more anodic potentials. This facilitates the reduction of $O_2^{=}$ ions, in particular the peroxide product of reaction [3], giving higher current densities. At low concentrations of CO_2 in the melt, the neutralization of oxide ions is slow, which causes a displacement of the local reduction potential of peroxide ions to more negative potentials. As a result, the peroxide product of reaction [5] is not further reduced, leading to lower current densities. In the mass-transfer control region, the neutralization reaction exerts less influence on the limiting currents. The limiting current densities then depend predominantly on the bulk concentration of $O_2^{=}$ and $O^{=}$ ions in the melt. From the equilibrium expressions in Eq. [8] and [9], these concentrations depend negatively on the partial pressure of CO_2. Therefore, high CO_2 concentrations result in lower limiting currents, whereas low CO_2 concentrations result in higher limiting currents.

The simulated effect of changes in the autocatalytic reaction rate (*i.e.*, enhancement of dioxygen ion concentration unneutralized as $O^{=}$ increases in the presence of molecular oxygen) on the polarization curves is shown in Fig. 6 by allowing the molecular concentration outside of the diffusion layer to vary, simulating the porous electrode case. The enhancement in current density is particularly promi-

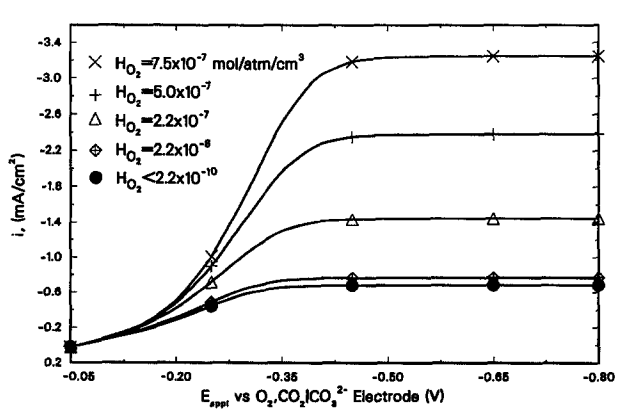

Fig. 3. Effect of physical solubility of oxygen on the steady-state polarization in (62:38) Li/K carbonate melt.

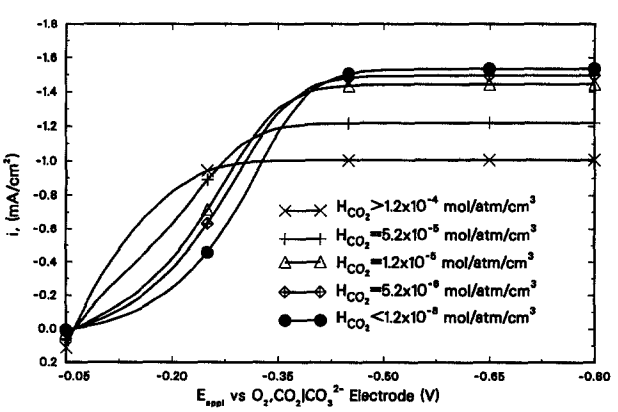

Fig. 5. Effect of carbon dioxide solubility on the steady-state polarization curves in (62:38) Li/K carbonate melt.

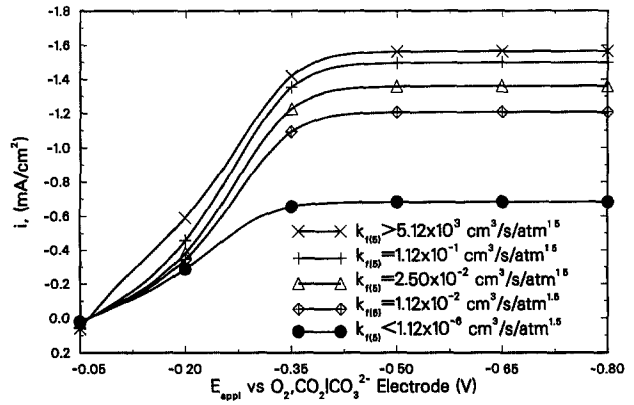

Fig. 6. Effect of autocatalytic reaction rate constant in Eq. [5] on the steady-state polarization curves in (62:38) Li/K carbonate melt. (H_{O_2} = 10^{-7} mol/atm/cm³).

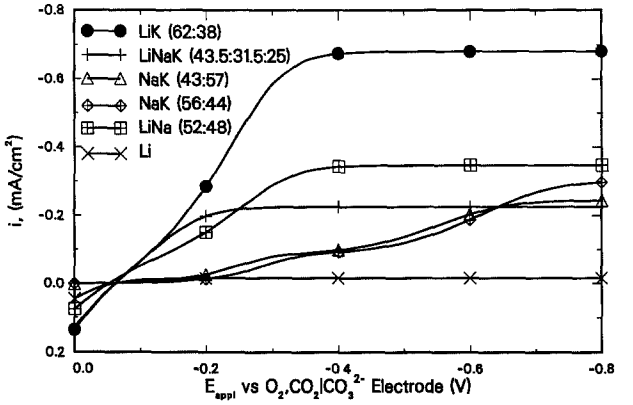

Fig. 8. Steady-state polarization curves in various carbonate melts in the absence of physically dissolved oxygen.

nent in the mass-transfer limiting region, and less so in the near-reversible region. High rates of the autocatalytic reaction, Eq. [5], favor the consumption of $O^=$ ions and the formation of O_2^- species in the melt. The O_2^- from reaction [5] is reduced in reaction [3], thus enhancing the current density. On the other hand, a consumption of oxide ions in reaction [5] results in a lowering of the local reduction potential for peroxide in Eq. [4], so that the increased amount of $O_2^=$ formed via reaction [3] is further reduced in reaction [4], giving an increase in current density. The overall effect is a significant enhancement of the current density at high rates via the autocatalytic reaction, which should be important in porous electrodes.

Figure 7 shows the effect of varying the rate of the oxide neutralization reaction on the polarization curves. These are characterized at high neutralization rate constant values by a current density enhancement in the kinetic control region and a corresponding decrease in the mass-transfer control region. The reverse situation would be observed at low neutralization rate constant values. Hence, if the neutralization reaction is slow and possibly rate-determining, overpotential in the kinetic control region will be considerable. As expected, the effect of the neutralization rate constant on the polarization curves is similar to that of CO_2 concentration. However, there is less variation in the overall range of current density in this case than would be expected if the concentration of CO_2 is allowed to vary.

The simulated polarization curves in various carbonate mixtures (Fig. 8 and 9) illustrate the effect of the cations present in the melt. The partial pressures of O_2/CO_2 are assumed to be the same level for all melt compositions. As a first-order estimate, the kinetic parameters were assumed to be the same for each melt except in $LiCO_3$ where only $O_2^=$ is the dissolved dioxygen ion. Figure 8 shows the case where dissolved molecular O_2 is negligible outside of the diffusion layer region, whereas Fig. 9 corresponds to the case where dissolved molecular O_2 is present. Both groups

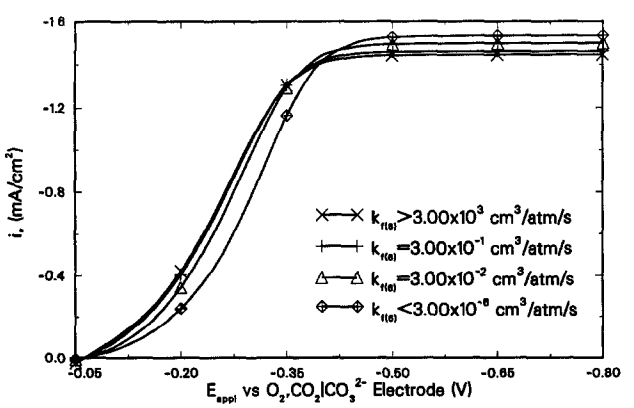

Fig. 7. Effect of oxide recombination reaction rate constant in Eq. [6] on the steady-state polarization curves in (62:38) Li/K carbonate melt. (H_{O_2} = 10^{-7}) mol/atm/cm³.

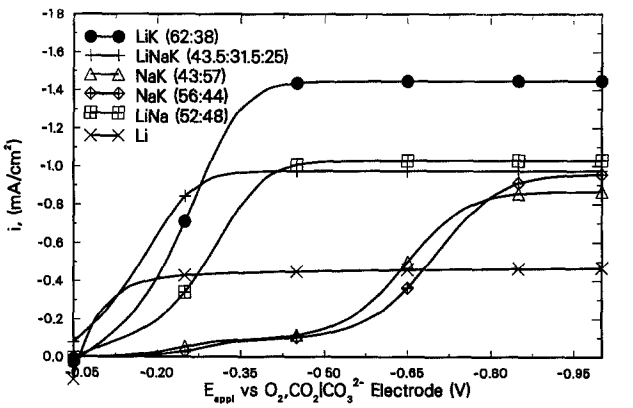

Fig. 9. Steady-state polarization curves in various carbonate melts in the presence of physically dissolved oxygen. (H_{O_2} = 10^{-7} mol/atm/cm³).

of polarization curves are similar; the major difference is the expected enhancement of the current densities for the latter case. The curves indicate that polarization of the MCFC cathode is dependent on the melt composition. As expected, the polarization curve in Li_2CO_3 shows only one limiting current, whereas those for other melts appear to show two limiting current regions; the first occurs near the open-circuit potential and corresponds to the reduction of $O_2^=$ species, the second occurs in the more cathodic potential region corresponding to the reduction of O_2^-. The first limiting current is not well defined in most cases and overlaps the second limiting current, as in the Li/K melt. However, two distinct limiting current regions can be observed in Na/K carbonate melts, in agreement with the results of Appleby and Nicholson in Li/K, Na/K, and Li carbonate melts (2-4).

Thermodynamic calculations indicate the equilibrium concentration of O_2^- is in the order K > Na > Li, whereas the concentration of $O^=$ is the reverse. Thus, K- or Na-rich melts produce the highest concentration of O_2^-. It is apparent that the higher the concentration of O_2^- in the melt, the higher is the limiting current density. Consequently, the Li_2CO_3 melt, where only $O_2^=$ is present, will show the lowest limiting current density. Thermodynamic calculations also indicate that reduction of $O_2^=$ ions occurs at more anodic potentials than that for O_2^-. Hence, kinetics near the reversible potential region are more dependent on $O_2^=$ ion concentration. Examination of the simulated polarization curves in Fig. 8 and 9 indicate that Li/K, Li/Na/K, Li/Na, and pure Li (Li-rich) melts should yield the best kinetic performance (lower overpotentials) in this region, where fuel cells normally operate.

Figures 10 and 11 show the effect of changing cation composition on the polarization curve in Li/K melts. In general, the electrolyte composition exhibits the same behavior in the presence or absence of dissolved oxygen outside of the diffusion layer region. Improved kinetics in the

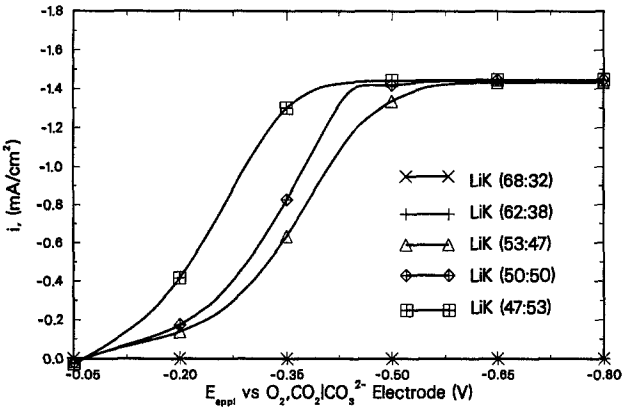

Fig. 10. Effect of cation concentration on the steady-state polarization curves of Li/K carbonate melt in the presence of physically dissolved oxygen. ($H_{O_2} = 10^{-7}$ mol/atm/cm^3).

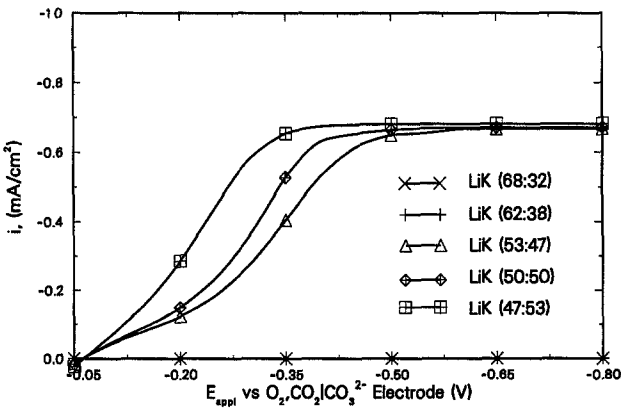

Fig. 11. Effect of cation concentration on the steady-state polarization curves in Li/K carbonate melt in the absence of physically dissolved oxygen.

near-reversible are observed with increasing Li-content, whereas the limiting currents do not vary significantly. These results are in general agreement with one set of fuel cell performance data results for melts of various compositions (23), however other analyses show discrepant results.

Finally, a sensitivity analysis similar to that reported earlier (24) was carried out for this system. The most sensitive parameters were found to be the apparent transfer coefficients, followed by the exchange current densities and the reaction rate constants; the least sensitive parameters were the diffusion coefficients of reacting species.

Conclusions

Mathematical modeling shows that the polarization curves for oxygen reduction in carbonate melts should be significantly affected by the concentrations of dissolved CO_2 and O_2 outside of the diffusion layer in the melt as well as by changes in the rates of the autocatalytic ($O_2 + 2\ O^=$) and neutralization ($CO_2 + O^=$) reactions. Simulation for different cation mixtures indicates that melts with high Li-content should yield the highest kinetic rates.

At present, experimental observations for comparison with the model simulations in this work are generally lacking. It is hoped that experiments on microelectrodes and ultrathin porous electrodes in various carbonate melts currently in progress in the authors' laboratory will lend support to the conclusions drawn from this work.

Acknowledgments

This work was supported by DOE (Grant No. DE-FG22-87PC79931) and by the Electric Power Research Institute.

Manuscript submitted May 30, 1989; revised manuscript received Jan. 20, 1990.

Texas A&M University assisted in meeting the publication costs of this article.

APPENDIX

Derivation of Kinetic Expression for the Electrode Reactions

The kinetic rate equations for reactions [3] and [4] are derived separately and then combined to obtain the overall rate equation at the electrode. For example, to derive the rate equation for reaction [4], the reaction is assumed to proceed by a sequence of elementary steps as outlined below

$$O_2^= + e^- \rightleftharpoons O^= + O^- \quad \text{(rds)} \qquad [4a]$$

$$O^- + e^- \rightleftharpoons O^= \qquad [4b]$$

$$O_2^= + 2e^- \rightleftharpoons 2\ O^= \qquad [4]$$

where Eq. [3a] is taken to be the rate-determining step (rds). The following assumptions were made to facilitate the derivation of the kinetic expression for the current density; (*i*) the rates of the elementary steps prior to and after the rds are high enough to be in quasi-equilibrium; (*ii*) the coverage of the electrode surface by adsorbed species is low, (*iii*) double layer effects are negligible, and (*iv*) the electrolyte behaves as an ideal solution.

The rate expression for the rds in Eq. [4a] can be expressed by the equation

$$\frac{i_{4a}}{n_{4a}\mathbf{F}} = k_{4a}c_{O^=,o}c_{O^-,o}\exp\left(\frac{\beta\mathbf{F}}{RT}V\right) - k_{-4a}c_{O_2^=,o}\exp\left(-\frac{1-\beta)\mathbf{F}}{RT}V\right) \qquad [A\text{-}1]$$

where V is the potential difference between the electrode and the adjacent solution

$$V = \Phi_{met} - \Phi_o \qquad [A\text{-}2]$$

Application of the quasi-equilibrium assumption to Eq. [4b] gives rise to the following expressions

$$K_{4b} = k_{4b}/k_{-4b} = \frac{c_{O^-}}{c_{O^=,o}}\exp\left(-\frac{\mathbf{F}}{RT}V\right) \qquad [A\text{-}3]$$

which is substituted into Eq. [A-2] for $c_{\bar{O}}$ to give

$$i_{4a} = k_4 c_{O^=,o}^2\exp\left(\frac{\alpha_{a,4}\mathbf{F}}{RT}V\right) - k_{-4}c_{O_2^=,o}\exp\left(-\frac{\alpha_{c,4}\mathbf{F}}{RT}V\right) \qquad [A\text{-}4]$$

where $k_4 = n_{4a}k_{4a}K_{4b}$ and $k_{-4} = n_{4a}\ k_{-4a}$, and where $\alpha_{a,4} = 1 + \beta$ and $\alpha_{c,4} = (1 - \beta)$. It must be noted that

$$\alpha_{a,4} + \alpha_{c,4} = n_4 = 2 \qquad [A\text{-}5]$$

where n_4 is the total number of electrons transferred in reaction [4]. At equilibrium, $i_4 = 0.0$ and the potential V becomes equal to the Nernst or equilibrium potential, $V'_{o,3}$. That is

$$i_4 = 0 = k_4 c_{O^=,o}^2\exp\left(\frac{\alpha_{a,4}\mathbf{F}}{RT}V'_{o,4}\right) - k_{-4}c_{O_2^=,o}\exp\left(-\frac{\alpha_{c,4}\mathbf{F}}{RT}V'_{o,4}\right) \qquad [A\text{-}6]$$

The exchange current density corresponding to this surface equilibrium composition, $i'_{o,4}$, is defined as

$$i'_{o,4} = k_4 c_{O^=,o}^2\exp\left(\frac{\alpha_{a,4}\mathbf{F}}{RT}V'_{o,4}\right) = k_{-4}c_{O_2^=,o}\exp\left(-\frac{\alpha_{c,4}\mathbf{F}}{RT}V'_{o,4}\right) \qquad [A\text{-}7]$$

Substitution of Eq. [A-7] into Eq. [A-4] yields

$$\frac{i_4}{i'_{o,4}} = \exp\left[\frac{\alpha_{a,4}\mathbf{F}}{RT}(V - V'_{o,4})\right] - \exp\left[-\frac{\alpha_{c,4}\mathbf{F}}{RT}(V - V'_{o,4})\right] \qquad [A\text{-}8]$$

Further manipulation of Eq. [A-7] results in an alternate expression for $i'_{o,4}$

$$i'_{o,4} = k_4^{(1-\alpha_{a,4}/n_4)} k_{-3}^{\alpha_{a,4}/n_4} c_{O_2^=,o}^{2(1-\alpha_{a,4}/n_4)} c_{O_2^=,o}^{\alpha_{a,4}/n_4} \quad [A\text{-}9]$$

The rate constants in Eq. [A-9] are unknown and they can be eliminated by assuming that the exchange current density is known at some reference concentration, $c_{i,ref}$, that is

$$\frac{i'_{o,4}}{i_{o4,ref}} = \left(\frac{c_{O^=,o}}{c_{O^=,ref}}\right)^{(1-\alpha_{a,4}/n_4)} \left(\frac{c_{O_2^=,o}}{c_{O_2^=,ref}}\right)^{\alpha_{a,4}/n_4} \quad [A\text{-}10]$$

The equilibrium relation from Eq. [1] in Li-K melt is given as (5)

$$C_{O_2^=,ref} = K_1 \frac{p_{O_2,ref}^{1/2}}{p_{CO_2,ref}} \quad [A\text{-}11]$$

and from Eq. [6] under equilibrium conditions

$$C_{O^=,ref} = K_6 p_{O_2,ref}^{-1} \quad [A\text{-}12]$$

Therefore the exchange current density can be expressed in terms of the partial pressures of O_2 and CO_2 as follows

$$i'_{o4,ref} = k'_4 p_{O_2,ref}^{1/2(\alpha_{a,4}/n_4)} p_{CO_2,ref}^{-(2-\alpha_{a,4}/n_4)} \quad [A\text{-}13]$$

The current density expression for reaction [4] can be written in terms of $i_{o4,ref}$ by substituting Eq. [A-10] into Eq. [A-8]

$$\frac{i_4}{i_{o4,ref}} = \left(\frac{c_{O^=,o}}{c_{O^=,ref}}\right)^{(1-\alpha_{a,4}/n_4)} \exp\left[\frac{\alpha_{a,4}\mathbf{F}}{RT}(V - V'_{o,4})\right] - \left(\frac{c_{O_2^=,o}}{c_{O_2^=,ref}}\right)^{\alpha_{a,4}/n_4} \exp\left[\frac{-\alpha_{c,4}\mathbf{F}}{RT}(V - V'_{o,4})\right] \quad [A\text{-}14]$$

The open-circuit potential for reaction j evaluated at the surface concentrations, $c_{i,o}$ is defined as

$$V'_{o,j} = U_j^\theta - U_{re}^\theta - \frac{RT}{n\mathbf{F}} \sum_i s_{ij} \ln\left(\frac{c_{i,o}}{\rho_o}\right) + \frac{RT}{n_{re}\mathbf{F}} \sum_i s_{i,re} \ln\left(\frac{c_{i,re}}{\rho_o}\right) \quad [A\text{-}15]$$

when reaction j is written in the form

$$\sum_i s_{ij} M^{z_i} \rightarrow n_j e^- \quad [A\text{-}16]$$

From Eq. [A-15], the open-circuit potential in terms of reference concentrations, $c_{i,ref}$ is as follows

$$U_{j,ref} = U_j^\theta - U_{re}^\theta - \frac{RT}{n_j\mathbf{F}} \sum_i s_{ij} \ln\left(\frac{c_{i,ref}}{\rho_o}\right) + \frac{RT}{n_{re}\mathbf{F}} \sum_i s_{i,re} \ln\left(\frac{c_{i,re}}{\rho_o}\right) \quad [A\text{-}17]$$

Substitution of Eq. [A-17] into Eq. [A-15] yields

$$V'_{oj} = U_{j,ref} - \frac{RT}{n_j\mathbf{F}} \sum_i s_{ij} \ln\left(\frac{c_{i,o}}{c_{i,ref}}\right) \quad [A\text{-}18]$$

In terms of reaction [4], the open-circuit potential is given by

$$V'_{o,4} = U_{4,ref} - \frac{RT}{n_4\mathbf{F}} \ln\left[\left(\frac{c_{O^=,o}}{c_{O^=,ref}}\right)^2 \left(\frac{c_{O_2^=,ref}}{c_{O_2^=,o}}\right)\right] \quad [A\text{-}19]$$

and therefore

$$(V - V'_{o,4}) = V - U_{4,ref} - \frac{RT}{n_2\mathbf{F}} \ln\left[\left(\frac{c_{O^=,o}}{c_{O^=,ref}}\right)^2 \left(\frac{c_{O_2^=,ref}}{c_{O_2^=,o}}\right)\right] \quad [A\text{-}20]$$

where

$$U_{4,ref} = U_4^\theta - U_{re}^\theta - \frac{RT}{n_4\mathbf{F}} \ln\left[\left(\frac{c_{O_4^=,ref}}{\rho_o}\right)\left(\frac{\rho_o}{c_{O_4^=,ref}}\right)\right] + \frac{RT}{n_{re}\mathbf{F}} \sum_i s_{i,re} \ln\left(\frac{c_{i,re}}{\rho_o}\right) \quad [A\text{-}21]$$

Equation [A-2] is substituted for V in Eq. [A-20] and the result is substituted into Eq. [A-14]. With further simplification and rearrangement, the final expression for the current density is

$$i_4 = i_{o4,ref}\left[\left(\frac{c_{O^=,o}}{c_{O^=,ref}}\right)^2 \exp\left(\frac{\alpha_{a,4}\mathbf{F}}{RT}\eta_4\right) - \left(\frac{c_{O_2^=,o}}{c_{O_2^=,ref}}\right) \exp\left(\frac{-\alpha_{c,4}\mathbf{F}}{RT}\eta_4\right)\right] \quad [A\text{-}22]$$

where the overpotential, η_4 is given by

$$\eta_4 = \Phi_{met} - \Phi_o - U_{4,ref} \quad [A\text{-}23]$$

The corresponding current density expression for reaction [3] is given by

$$i_3 = i_{o3,ref}\left[\left(\frac{c_{O_2^=,o}}{c_{O_2^=,ref}}\right) \exp\left(\frac{\alpha_{a,3}\mathbf{F}}{RT}\eta_4\right) - \left(\frac{c_{O_2^=,o}}{c_{O_2^=,ref}}\right) \exp\left(\frac{-\alpha_{c,3}\mathbf{F}}{RT}\eta_3\right)\right] \quad [A\text{-}24]$$

where

$$\eta_3 = \Phi_{met} - \Phi_o - U_{3,ref} \quad [A\text{-}25]$$

and the exchange current density with respect to the partial pressures of O_2 and CO_2 is given by

$$i_{o3,ref} = k'_4 p_{O_2,ref}^{3/4\alpha_{a,4}/n_4} p_{CO_2,ref}^{-2(1-3/4\alpha_{a,4}/n_4)} \quad [A\text{-}26]$$

Experimentally, the measured potential is generally referred to as the applied potential, E_{appl}, and is the potential difference between working electrode, Φ_{met}, and the potential at the reference electrode, Φ_{re}, as expressed below

$$E_{appl} = \Phi_{met} - \Phi_{re} \quad [A\text{-}27]$$

$$\eta_j = \Phi_{met} - \Phi_{re} - (\Phi_0 - \Phi_{re}) - U_{j,ref} = E_{appl} - (\Phi_0 - \Phi_{re}) - U_{j,ref} \quad [A\text{-}28]$$

where $(\Phi_o - \Phi_{re})$ is the ohmic potential drop in the solution. Consequently, the measured overpotential is

$$\eta = \Phi_{met} - \Phi_{re} - U_{ocp} \quad [A\text{-}29]$$

where U_{ocp} is the open-circuit potential.

LIST OF SYMBOLS

c_i	concentration of species i, mol/cm^3
D_i	diffusion coefficient of species i, cm^2/s
D_R	diffusion coefficient of limiting reactant, cm^2/s
E_{appl}	applied electrode potential, V
$\mathbf{F}$	Faraday constant, 96,487 C/mol
H_i	Henry's constant for species i
i_j	local current density due to reaction j, A/cm^2
$i_{o,j}$	exchange current density due to reaction j at surface concentrations, A/cm^2
$i_{oj,ref}$	exchange current density due to reaction j at reference concentrations, A/cm^2
i	total current density, A/cm^2
K_j	equilibrium constant for homogeneous reaction j in the bulk solution
$k_b(j)$	backward rate constant for homogeneous reaction, j
$k_f(j)$	forward rate constant for homogeneous reaction, j
k_{-j}	backward rate constant for reaction j on the electrode
k_j	forward rate constant for reaction j on the electrode
$\mathbf{N}_i$	flux of species i, mol/cm^2-s
N	number of species in the solution
n_j	number of electrons transferred in reaction j
p_i	partial pressure of component i in gas mixture, atm.
R	universal gas constant, 8.314 J/mol-K
R_i	rate of disappearance of species i by a homogeneous reaction in the solution, mol/s
rpm	revolution per minute
s_{ij}	stoichiometric coefficient of species i in reaction j
T	absolute temperature, K
u_i	mobility of species i, cm^2-mol/J-s
U_j	theoretical open-circuit potential for reaction j, V
U_j^θ	standard electrode potential for reaction j, V
U_{ocp}	open-circuit potential with respect to the reference O_2 electrode

U^{θ}_{re} standard potential of the reference electrode on the absolute thermodynamic scale, V
V potential difference between metal of the working electrode and the solution just outside the diffuse double layer, V
$V'_{o,j}$ value of V when working electrode is at equilibrium in a solution of composition equivalent to that adjacent to the electrode surface
v bulk fluid velocity, cm/s
y normal coordinate into the solution from the electrode surface, cm
z_i charge of species i

Greek

$\alpha_{a,j}$ apparent anodic transfer coefficient for reaction j
$\alpha_{c,j}$ apparent cathodic transfer coefficient for reaction j
β true transfer coefficient
δ_D diffusion layer thickness, cm
ρ_o density of solution, kg/cm^3
Φ potential in the solution, V
Φ_{met} potential of working electrode, V
Φ_{re} potential in the bulk solution at the location of the reference electrode, V
η_j overpotential of reaction j, V
μ_i stoichiometric coefficient of species i in a homogeneous reaction
ν kinematic viscosity, cm^2/s
ξ dimensionless distance, y/δ_D
Ω rotation speed, rad/s

Subscripts

o at the electrode surface
j reaction, j
re reference electrode
ref reference conditions
bulk in the bulk solution

REFERENCES

1. A. J. Appleby and S. Nicholson, *J. Electroanal. Chem.*, **38,** App. 15 (1972).
2. A. J. Appleby and S. Nicholson, *ibid.*, **53,** 105 (1974).
3. A. J. Appleby and S. Nicholson, *ibid.*, **83,** 309 (1977).
4. A. J. Appleby and S. Nicholson, *ibid.*, **112,** 71 (1980).
5. S. W. Smith, W. M. Vogel, and S. Kapelner, *This Journal,* **129,** 1668 (1982).
6. W. M. Vogel, S. W. Smith, and S. Bregoli, *ibid.*, **130,** 574 (1983).
7. B. K. Andersen, Ph.D. Dissertation, Technical University of Denmark, Lyngby, Denmark (1975).
8. C.-Y. Yuh, Ph.D. Thesis, Illinois Institute of Technology, Chicago, IL (1985).
9. J. R. Selman, *Energy,* **16,** 153 (1984).
10. S.-H. Lu, Ph.D. Thesis, Illinois Institute of Technology, Chicago, IL (1985).
11. N. I. Uchida, T. Nishina, Y. Mugikura, and K. Itaya, *J. Electroanal. Chem.*, **206,** 229 (1986).
12. J. Winnick and P. N. Ross, *This Journal,* **128,** 991 (1981).
13. G. Wilemski, *ibid.*, **130,** 117 (1983).
14. H. R. Kunz, L. J. Bregoli, and S. T. Szymanski, *ibid.*, **131,** 2815 (1984).
15. A. Borucka and C. M. Sugiyama, *Electrochim. Acta,* **13,** 1807 (1968).
16. S. H. White and U. M. Twardoch, *ibid.*, **27,** 1599 (1982).
17. P. K. Adanuvor, R. E. White, and S. E. Lorimer, *This Journal,* **134,** 625 (1987).
18. J. S. Newman, "Electrochemical Systems," Prentice-Hall, Inc., Englewood Cliffs, NJ (1973).
19. D. R. Stull and H. Prophet, "The JANAF Tables," 2nd ed., NBS, Washington, DC (1971).
20. N. Godshall, Ph.D. Thesis Stanford University, Stanford, CA (1980).
21. J. Newman, *Ind. Eng. Chem. Fundam.*, **5,** 525 (1966).
22. S. H. White and U. M. Twardoch, in "Molten Carbonate Fuel Cell Technology," (PV 84-13) J. R. Selman and T. D. Claar, Editors, p. 434, The Electrochemical Society Softbound Proceedings Series, Pennington, NJ (1984).
23. H. C. Maru, L. Paetsch, and A. Pigeaud, *ibid.*, p. 20.
24. P. K. Adanuvor and R. E. White, *This Journal,* **135,** 1887 (1988).

Analysis of a Pulsed-Plasma Chemical Vapor Deposition Reactor with Recycle

Sang-Kyu Park* and Demetre J. Economou**

Department of Chemical Engineering, University of Houston, Houston, Texas 77204-4792

ABSTRACT

A simplified model for a time-dependent plasma-assisted chemical vapor deposition reactor was developed based on transport and reaction principles. The model equations were solved by the method of lines using collocation on finite elements for the spatial discretization. Emphasis was placed on the deposition rate and uniformity as a function of reactor operating conditions. A pulsed-plasma reactor was analyzed, and compared to a continuous-wave (CW) plasma reactor. Under conditions which would result in high depletion of the precursor gas in the CW reactor, the pulsed-plasma reactor yielded improved uniformity, albeit the deposition rate was reduced. The effect of a recycle stream on both the CW and pulsed-plasma reactors was also studied. For the CW reactor, recycle was most beneficial under conditions of low depletion of the precursor gas. For cases of intermediate depletion of the precursor gas, a CW reactor with recycle or a combination of pulsed-plasma and recycle can result in nearly uniform deposit without sacrificing the deposition rate. Analytic solutions were derived for the CW reactor with recycle, and for a well-mixed pulsed-plasma reactor. The results apply equally well to pulsed-plasma etching reactors conforming to the model assumptions and operating under corresponding conditions.

Plasma-assisted deposition and etching of thin solid films has emerged as a crucial step in the fabrication of microelectronic components (1), and is expected to become even more important in the future. In plasma processing, a low-pressure gas discharge is used to decompose an otherwise inert gas to produce reactive atoms and radicals. The reactive species interact with a substrate to deposit a thin film or to etch the substrate by forming volatile products (2).

Plasma-assisted chemical vapor deposition (PCVD) is used extensively to grow a variety of thin films including dielectrics (*e.g.*, SiO_2 and Si_3N_4) (3, 4), amorphous hydrogenated silicon a-Si:H (5), polymers (6), and more recently diamond (7). In particular, PCVD is the method of choice when low-temperature deposition is required. For example, PCVD is used to deposit a Si_3N_4 passivation layer over devices in which aluminum metallization prohibits the use of conventional high-temperature CVD methods.

Important goals of PCVD include high deposition rate and uniformity, and high quality of the deposited film.

* Electrochemical Society Student Member.
** Electrochemical Society Active Member.